

CHAPTER 90

NUMERICAL MODELING FOR WAVE ENERGY DISSIPATION WITHIN POROUS SUBMERGED BREAKWATERS OF IRREGULAR CROSS SECTION

George Z. Gu¹ and Hsiang Wang²

Abstract

In the design of a porous submerged breakwater, the maximum wave energy dissipation within the breakwater is desirable. To calculate the energy dissipation, the process is simulated numerically in this study using the Boundary Integral Element Method (BIEM). The breakwater is idealized as a homogeneous porous medium and the flow inside the breakwater is modeled by a non-linear porous flow model which is linearized iteratively based on the equivalent energy principle in the numerical model. To fully explore the advantage of BIEM, a boundary integral expression for wave energy dissipation developed in an earlier work by the authors is used to replace the traditional domain integral expression. As a result, the efficiency of the numerical model is greatly increased. The numerical model was run for a number of cases and the results show that the maximum wave energy dissipation can be achieved at a practical permeability level (or stone size). The good agreement between the numerical results and the experiment data for non-breaking waves indicates that the wave energy dissipation within porous breakwaters can be adequately predicted by the numerical model.

Introduction

Due to increasing demand for beach protection in recreational areas, submerged breakwaters may become more and more popular over traditional sub-aerial ones. The advantages of submerged breakwaters as compared to sub-aerial ones are of low cost, aesthetics (they do not block the view of the ocean) and effectiveness in triggering early breaking of the incident waves. More general, a low crest sub-aerial breakwater may become submerged during storm surge or after being damaged.

¹Dallas E & P Engineering, Mobil R & D Corp. 13777 Midway, Dallas TX 75244. Formerly with Coastal and Oceanographic Engineering Dept. University of Florida

²Professor, Coastal and Oceanographic Engineering Dept. of U. of Florida, Gainesville, FL, 32611

In the design of a porous submerged breakwater, one of the important aspects is to assess the energy dissipation within the structure due to turbulence and friction. Maximum energy dissipation (equivalently, minimum wave transmission) is usually desired.

The wave transmission, reflection and energy dissipation has been studied experimentally by Dick (1968), Dattatri (1978), Seelig (1980) and many other investigators. The measurements in these model tests were generally limited to the free surface oscillations on the weather and lee side of a submerged breakwater. As pointed out by Kobayashi et al. (1989), such measurements do not reveal the hydrodynamic processes over and within porous submerged breakwaters. In terms of theoretical modeling, a great deal of contributions have been made by Sollitt et al. (1972), Madsen (1974), Ijima et al. (1974), Sulisz, 1985 and others to the problem of wave interaction with sub-aerial porous breakwaters. Kobayashi (1989) successfully modeled the wave interaction with impermeable submerged breakwaters. However, the process of wave energy dissipation within porous submerged breakwaters has not been investigated thoroughly enough to guide practical designs.

In this paper, a numerical model using the Boundary Integral Element Method (BIEM) is developed to model wave interaction with porous submerged breakwaters. In general, wave attenuation over a porous submerged breakwater is affected by three mechanisms: reflection by the structure, breaking over the structure and damping due to percolation inside the porous structure. The wave energy dissipation are mainly caused by wave breaking and flow percolation. The main focus of this study is on the process of wave energy dissipation due to percolation.

The submerged breakwater is modeled as an infinitely long, shore parallel structure. The porous body of the structure is assumed to be a homogeneous porous medium, and described by the non-linear unsteady percolation model.

Governing Equations and Boundary Conditions

The computation domain of the problem consists of two sub-domains, the fluid domain and the domain(s) of the submerged porous media (more than one porous domain if the breakwater has multiple layers). In the fluid domain, the water is considered inviscid and incompressible. The flow induced by gravity waves is assumed irrotational. Thus, the governing equation in this domain, for the velocity potential function Φ , is the Laplace equation,

$$\nabla^2 \Phi = 0 \quad (1)$$

with fluid velocities being defined as

$$u = -\frac{\partial\Phi}{\partial x} \tag{2}$$

$$w = -\frac{\partial\Phi}{\partial z} \tag{3}$$

Further more we assume sinusoidal wave motion such that

$$\Phi = \phi e^{i\sigma t} \tag{4}$$

While in the porous domain, the viscosity of the fluid cannot be ignored since the flow is largely within the low Reynolds number region. The flow induced by sinusoidal linear waves can be described by the non-linear unsteady porous flow model used by Sollitt and Cross (1972)

$$-\frac{1}{\rho}\nabla P(x,y,z,t) = \sigma\left(\frac{1}{R} + i\beta + \frac{C_f}{\sqrt{\sigma\nu R}} |\vec{q}(x,y,z,t)|\right)\vec{q}(x,y,z,t) \tag{5}$$

or

$$-\frac{1}{\rho}\nabla p(x,y,z,t) = \sigma(f_1 + f_2 |\vec{q}|)\vec{q} \tag{6}$$

with

$$\Psi(x,y,z,t) = \psi(x,y,z)e^{i\sigma t}$$

$$f_1 = \frac{1}{R} + i\beta; \quad f_2 = \frac{C_f}{\sqrt{\sigma\nu R}}$$

where Ψ can be P or \vec{q} or any other wave field variable; $P(x,y,z,t)$ is the pore pressure function inside porous media; ν and ρ are the kinematic viscosity and the density of sea water, respectively; R is the permeability parameter defined as

$$R = \frac{\sigma K_p}{\nu}$$

K_p is the intrinsic permeability of the porous media, measured under the conditions of steady flows; it is empirically related to particle diameter by (Engelund, 1953)

$$K_p = \frac{n^2 d_s^2}{a_0 (1-n)^3} \tag{7}$$

where a_0 is an empirical constant and it is taken to be 570; n is the volumetric porosity; σ is the wave frequency; β is the inertial resistance parameter and C_f is a non-dimensional constant characterizing the non-linear resistance. In this study, $\beta = 4.6$ and $C_f = 1.0$, as determined by a seabed experiment (Gu and Wang, 1990, Gu, 1990); $\vec{q}(x,y,z,t)$ is the complex vector of discharge velocity in the porous medium.

Due to the mathematical difficulties in applying the non-linear model directly, the common practice is to linearize Eq.(6) such that

$$-\frac{1}{\rho}\nabla p = \sigma f_0 \vec{q} \tag{8}$$

where f_0 is the linearized resistance coefficient which is a constant for a particular problem. This coefficient can be obtained by using the principle of equal energy dissipation, as will be discussed later. At this point, we assume that f_0 is a known complex constant. Substitution of the above equation into the continuity equation gives the Laplace equation for p ,

$$\nabla^2 p = 0 \tag{9}$$

The boundary conditions for the fluid domain are:

$$\frac{\partial \phi}{\partial z} = \frac{\sigma^2}{g} \quad z = 0 \tag{10}$$

$$\frac{\partial \phi}{\partial n} = 0 \quad z = -h(x) \tag{11}$$

On the lateral boundary of lee side, $x = l'$,

$$\frac{\partial \phi}{\partial n} = \frac{\partial \phi}{\partial x} = -ik'\phi \quad \text{with} \quad gk' \tanh k'h' = \sigma^2 \tag{12}$$

where h' is the water depth at $x = l'$.

While on the lateral boundary of weather side, $x = -l$,

$$\frac{\partial \phi}{\partial n} = 2ik\phi_I - ik\phi \quad \text{with} \quad gk \tanh kh = \sigma^2 \tag{13}$$

in which ϕ_I is the incident wave potential and h is the water depth at $x = -l$. For the porous domain(s),

$$\frac{\partial p}{\partial n} = 0 \quad \text{on impermeable surface(s)} \tag{14}$$

$$\left. \begin{aligned} \rho \frac{\partial \phi}{\partial t} &= p \\ \frac{\partial \phi}{\partial n} &= -\frac{1}{\rho \sigma f_0} \frac{\partial p}{\partial n} \end{aligned} \right\} \text{between fluid and porous domains} \tag{15}$$

$$\left. \begin{aligned} p_i &= p_j \\ \left(\frac{1}{f_0} \frac{\partial p}{\partial n}\right)_i &= -\left(\frac{1}{f_0} \frac{\partial p}{\partial n}\right)_j \end{aligned} \right\} \text{between two different porous domains} \tag{16}$$

where i and j refer to different porous domain.

Numerical Formulation of Boundary Integral Element Method

The boundary value problem stated in the previous section is solved numerically using the boundary integral element method (BIEM or BEM) owing to the irregular geometries of porous submerged breakwaters. The method has been proved to be a powerful and convenient method for problems governed by the Laplace equation.

Under the assumption of continuous and second order differentiable, the wave potential function ϕ in the fluid domain D_1 bounded by a closed boundary C_1 can be expressed by

$$\alpha\phi(\mathbf{x}_0) = \oint_{C_1} [\phi(\mathbf{x}) \frac{\partial G}{\partial n}(\mathbf{x}_0, \mathbf{x}) - G(\mathbf{x}_0, \mathbf{x}) \frac{\partial \phi}{\partial n}(\mathbf{x})] ds \quad (17)$$

where $G(\mathbf{x}_0, \mathbf{x})$ is a free space Green's function and α is a coefficient depending on the position of point \mathbf{x}_0 , (α is 2π when \mathbf{x}_0 is an interior point and equals to the inner angle of the boundary when it is a boundary point); \mathbf{x}_0 is a point in the domain $D_1 \cap C_1$ and \mathbf{x} is a boundary point on C_1 . The free space Green's function for normal incident wave is

$$G(\mathbf{x}_0, \mathbf{x}) = \ln r(\mathbf{x}_0, \mathbf{x}) = \ln \sqrt{(x_0 - x)^2 + (z_0 - z)^2} \quad (18)$$

Discretizing the boundary C_1 into N segments, the Eq.(17) becomes

$$\alpha_i \phi_i(\mathbf{x}_{0i}) = \sum_{j=1}^N \int_{C_{1j}} \left[\frac{\phi(\mathbf{x})}{r(\mathbf{x}_{0i}, \mathbf{x})} \frac{\partial r(\mathbf{x}_{0i}, \mathbf{x})}{\partial n} - \ln r(\mathbf{x}_{0i}, \mathbf{x}) \phi_n(\mathbf{x}) \right] ds \quad (19)$$

To evaluate the integrals, the curving segments C_{1j} are replaced by straightline segments. Each segment is then modeled by a linear element which assumes a linear variation of ϕ and ϕ_n over the segment. The line integration over each element can be carried out by introducing an auxiliary coordinate system (Liggett and Liu, 1983).

By applying the boundary conditions given in the previous section, Eq.(19) yields a set of linear algebraic equations with unknowns of ϕ_i and ϕ_{ni} ($i=1,2, \dots N$). In matrix form, it can be expressed as

$$\begin{bmatrix} \mathbf{A}_1 & \mathbf{A}_2 \end{bmatrix} \begin{Bmatrix} \phi_f \\ \phi_c \end{Bmatrix} = \begin{bmatrix} \mathbf{B}_1 & \mathbf{B}_2 \end{bmatrix} \begin{Bmatrix} \phi_f \\ \phi_{nc} \end{Bmatrix} + \mathbf{b} \quad (20)$$

where \mathbf{A}_i and \mathbf{B}_i ($i = 1, 2$) are the known matrices determined purely by boundary geometries, ϕ_c and ϕ_{nc} are the vectors of the unknown potential function and its normal derivative on the interface (common) boundary, ϕ_f and ϕ_{nf} are the vectors of the unknown potential function and its normal derivative along the boundaries other than the interface (common) boundary,

b is the known vector containing ϕ_I resulting from the radiation boundary condition on the weather side lateral boundary.

In the porous domain, a similar expression can be derived by replacing ϕ with p in Eq.(19). Introducing $p_n = 0$ on impermeable boundaries and carrying out the same operations, the resulted matrix equation for p and p_n is

$$\begin{bmatrix} C_{11} & C_{12} \\ C_{21} & C_{22} \end{bmatrix} \begin{Bmatrix} \mathbf{p}_c \\ \mathbf{p}_b \end{Bmatrix} = \begin{pmatrix} \mathbf{D}_{11} \\ \mathbf{D}_{21} \end{pmatrix} \mathbf{p}_{nc} \tag{21}$$

where \mathbf{p}_c and \mathbf{p}_{nc} are the vectors of pressure function and its normal derivative along the common boundary and \mathbf{p}_b is the pressure vector on the impervious bottom of the porous domain.

Based on Eq.(21) and solving \mathbf{p}_{nc} in terms of \mathbf{p}_c by eliminating \mathbf{p}_b , a relationship between \mathbf{p}_{nc} and \mathbf{p}_c can be established

$$\mathbf{p}_{nc} = \mathbf{E} \mathbf{p}_c \tag{22}$$

with

$$\mathbf{E} = (\mathbf{D}_{11} - C_{12} C_{22}^{-1} \mathbf{D}_{21})^{-1} (C_{11} - C_{12} C_{22}^{-1} C_{21}) \tag{23}$$

Substitution of the matching conditions stated in Eq.(15) into Eq.(22) and then into Eq.(20) yields

$$\bar{\mathbf{A}} \phi = \mathbf{b} \tag{24}$$

with

$$\bar{\mathbf{A}} = [\mathbf{A}_1 - \mathbf{B}_1 \quad \mathbf{A}_2 + \frac{i}{f_0} \mathbf{E} \mathbf{B}_2]_{N \times N} \tag{25}$$

and

$$\phi = \begin{Bmatrix} \phi_f \\ \phi_c \end{Bmatrix}_{N \times 1} \tag{26}$$

This is a determinant equation with complex matrix elements and it can be readily solved by a complex equation solver if the linearized coefficient f_0 for the resistances in the porous flow model is given. Unfortunately, it is still an unknown at this point and has to be determined by the linearization process.

Linearization of The Non-linear Percolation Model

The principle for the linearization is the equivalent energy dissipation by both linear and non-linear systems, i.e.

$$(E_D)_l = (E_D)_{nl} \tag{27}$$

For the energy dissipation E_D within a control volume (domain) V of porous medium during the time period T , the traditional expression (Sollitt et al, 1972, Madsen, 1974 and Sulisz, 1985) is

$$E_D = \int_V \int_t^{t+T} \vec{F} \cdot \rho \vec{q} dt dv \tag{28}$$

where \vec{F} is the dissipative resistance per unit volume of the porous medium, which is a function of the spatial coordinates and the time.

Since the domain integral in Eq.(28) is very awkward for a boundary element model, an equivalent expression in the form of boundary integration has been developed (Gu and Wang, 1991, Gu, 1990):

$$E_D = -\frac{T}{2} \int_C p^* u_n, ds \tag{29}$$

Where C is the common boundary of the fluid and the porous domains and p^* is the complex conjugate of p and u_n is the velocity normal to C , which is different for the linearized and for the non-linear systems. The ‘.’ sign is used here because E_D is considered as a positive value.

The physical explanation of Eq.(29) is that the energy dissipation inside the porous domain in one wave period T is equal to the net energy flux into the domain in the same time period. By expressing the energy dissipation in such a boundary integral, the advantage of BIEM can be well explored.

Equating $(E_D)_l$ to $(E_D)_{nl}$ and taking approximately $|\vec{q}| \simeq |p_n / \rho \sigma f_0|$, the linearized coefficient f_0 can be found to be

$$f_0 = \frac{\int_C p_n p^* ds}{\int_C \frac{p_n p^*}{f_1 + f_2 |p_n / \rho \sigma f_0|} ds} \tag{30}$$

Equation (30) can be easily solved by iteration.

Numerical Results

As an example, two submerged breakwaters are computed with the model. One breakwater is made of concrete, therefore impermeable, and the other one is made of quarry stones of $d_s = 0.4$ meters. The dimensions and the wave conditions are identical for both structures. The crest of the breakwater is 12 meters wide with 1.6 meter submergence in a water of 4.6 meters deep. The slopes are 1:1.5 on both sides. The wave envelopes and the waves at $t=0$ are shown in Fig. 1. Comparing the two wave envelopes, it is obvious that the transmitted wave height by the permeable breakwater is less than that by the concrete one due to wave energy dissipation inside the breakwater. The dissipation is $1.0 - K_T^2 - K_R^2 = 29\%$ of the total wave energy.

Fig. 2 illustrates the transmission and reflection coefficients for a submerged porous breakwater with a scale of 1:20 of the one in Fig. 1. In Fig. 2 the coefficients are plotted against the permeability parameter R for four

different wave heights, $H = 2.0, 4.0, 6.0$ and 8.0 cm. The wave period is kept constant, at $T = 1.2$ s. The transmission coefficient is shown to have a minimum value for each wave height for a particular stone size (around $R \approx 1.0$, $d_s \approx 1.6$ cm). A close examination of the resistances showed that this minimum transmission or maximum energy dissipation is achieved when the dissipative resistance (velocity related) is equal to the non-dissipative (acceleration related) resistance.

It can be observed in the figure that the permeability corresponding to the minimum transmission increases with increasing incident wave height, whereas the energy dissipation rate remains more or less the same. When the permeability (or equivalently the stone size) is greater than a certain value, say $R = 10.0$ ($\log R = 1.0$), the wave transmission decreases with increasing wave height. This means that larger stones are more effective for protection against storms. The curves in Fig. 2 also implies that the stone size (or permeability) should be large enough so that it will not fall to the left of the trough for the design wave height.

Laboratory Experiment

The experiment was conducted in the Coastal Engineering Laboratory of Coastal and Oceanographic Engineering Department, University of Florida. The tank was 25 meters long, 0.6 meters wide and 1.7 meters deep with glass walls on both sides. The wave maker is of piston type furnished with an absorbing system which was designed to absorb the wave energy reflected back to the piston. The tank is also equipped with a motorized rail cart on the top to facilitate wave envelope measurements.

The model of the porous submerged breakwater was of trapezoidal shape made of river gravel of $d_{50} = 0.93$ cm. It has the same configuration as the one shown in Fig. 1 with a scale factor of 1:20. The measurements were concentrated on wave reflection and transmission, although the wave envelope over the breakwater crest was also measured.

In the experiment, the measurements of transmission and reflection coefficients were carried out for 9 wave periods ranging from $T = 0.642$ seconds to $T = 1.778$ seconds with several different wave heights for each wave period. Both non-breaking and breaking waves were tested. Here 'breaking' refers to white caps over the breakwater crest, not breaking of incident waves.

It was observed in the experiment that higher order harmonics occur on the down wave side of the breakwater model, as opposed to monochromatic waves predicted by the numerical model. Fig 3 is the energy spectrum of a typical transmitted wave record. The data also showed that in general, the

wave energy of the first three modes accounts for more than 98% of the total transmitted wave energy.

In order to compare with the numerical results which is based upon the energy balance of the fundamental waves, an equivalent height for a transmitted wave was defined for the experimental data by summing the wave energy of the harmonics i.e.

$$(H_t)_{eq} = \sqrt{\sum_{i=1}^N (H_t)_i^2} \approx \sqrt{\frac{8}{\gamma} E} \quad (31)$$

where $(H_t)_i$ is the wave height of the i -th order harmonic wave, which can be determined by the corresponding spike area of the spectrum diagram and E is the total energy per unit area of all the harmonics.

Figure 4 and 5 are the plots of the transmitted and reflected wave heights versus the corresponding incident wave heights. Also plotted are the predicted values by the numerical model. The agreement between the data and the prediction is reasonably good for transmitted waves before breaking occurs. Although the agreement for the reflected waves is not as good, it is not difficult to envision a good agreement for the energy dissipation ($E_D = H_i^2 - H_t^2 - H_r^2$), because of small amplitude for the reflected waves. From Fig. 4 and 5, it is clear that the breaking occurs when the incident wave height is about $H_i = 4.2$ cm. After the waves break over the crest, the numerical model limited to non-breaking waves apparently over estimates the transmitted wave heights. When the incident wave height is over the breaking threshold (4.2 cm for this case), the transmitted wave height in the experiment changes only slightly, if at all, with the increasing incident wave height. The reflected waves are not noticeably affected by the breaking over the crest.

In Fig. 6, the wave envelopes (normalized by the incident wave heights) predicted by the model are compared with those of measured in the experiment for the case of $T = 0.856$ seconds; both non-breaking and breaking cases are shown. In the non-breaking case, although the measured wave envelope above the breakwater crest is shifted slightly upward, the numerical model is able to predict, with sufficient accuracy, both the variation patterns and the magnitudes of the wave heights (the distances between the two envelope profiles). Good agreement was also found for the non-breaking portion of the breaking wave cases. The upward shift of the mean water level in the data is believed to be caused by set-up over the crest.

Conclusions

An efficient numerical algorithm using boundary integral method was developed to compute the energy dissipation inside submerged rubble-mound breakwaters of irregular cross sections. The porous flow model simulating the porous breakwaters includes both the velocity induced linear and non-linear resistances as well as the acceleration induced inertial resistance. The replacement of the domain integral expression for the energy dissipation—commonly required by the linearization of the porous flow model—by a boundary integral is a key element in achieving the efficient numerical algorithm.

The numerical results show that under a given wave condition the rate of energy dissipation in a porous structure has a well defined maximum when the dissipative (velocity related) resistance is equal to the non-dissipative (acceleration related) resistance. It is shown that porous submerged breakwaters, if designed properly, could be more effective than impervious ones with same dimensions. It is also shown that large stones (or high permeability) is more effective for protection against storms than small stones.

Laboratory experiments were also conducted under both non-breaking and breaking wave conditions. The energy dissipation and wave envelope over the crest predicted by the model agree well with the experiments for non-breaking cases and for the non-breaking portion of the breaking cases. For breaking waves, the crest submergence of the breakwater appears to play a dominant role in limiting the wave energy transmission.

References

1. Dattatri, J., Raman, H., and Shankar, N.J., 1978, Performance Characteristics of Submerged Breakwaters, *Proc. 16th Coastal Eng. Conf.*, ASCE, 2153-2171.
2. Dick, T.M., and Brebner, A., 1968, Solid and Permeable Submerged Breakwaters, *Proc. 11th Coastal Eng. Conf.*, ASCE, 1141-1158.
3. Engelund, F., 1953, On the Laminar and Turbulent Flows of Ground Water Through Homogeneous Sand. *Trans. of the Danish Academy of Technical Sciences* **3**, No. 4.
4. Gu, Z., 1990, Water Wave Interaction with Porous Structures of Irregular Cross Sections. *PhD Dissertation, University of Florida*.
5. Gu, Z. and Wang, H, 1991, Gravity Waves over Porous Bottoms. *Coastal Engineering* **21**, 497-524.
6. Ijima, T., Chou., C.R., and Yoshida, A., 1976, Method of Analysis for Two-Dimensional Water Wave Problems, *Proc. 15th Coastal Eng. Conf.*, ASCE, 2717-2736.

7. Kobayashi, N. and Wurjanto, A., 1989, Wave Transmission over Submerged Breakwaters, *J. of the Waterways, Port, Coastal, and Ocean Engineering*, ASCE, Vol. 115, No.5.
8. Liggett., J.A., and Liu, P.L-F., 1983, *The Boundary Integral Equation Method for Porous Media Flow*, George Allen & Unwin Ltd.
9. Madsen, O.S., 1974, Wave Transmission through Porous Structures, *J. of the Waterways Harbors and Coastal Engineering Div.*, ASCE, Vol. 100, No.WW3.
10. Seelig, W.N., 1980, Two-Dimensional Tests of Wave Transmission and Reflection Characteristics of Laboratory Breakwaters, *Technical Report 80-1*, U.S. Army, Corps of Engineers, CERC., Ft. Belvoir, Virginia.
11. Sollitt, C.K., and Cross, R.H., 1972, Wave Transmission through Permeable Breakwaters. *Proc. 13th Coastal Eng. Conf., ASCE III*, 1827-1846.
12. Sulisz, W., 1985, Wave Reflection and Transmission at Permeable Breakwaters of Arbitrary Cross Section, *Coastal Engineering* Vol. 9, 371-386.
13. Wang, H. and Gu, Z., 1988. Gravity Waves over Porous Bottom. 2nd International Symp. on Wave Research and Coastal Engineering, pp. 1-21.

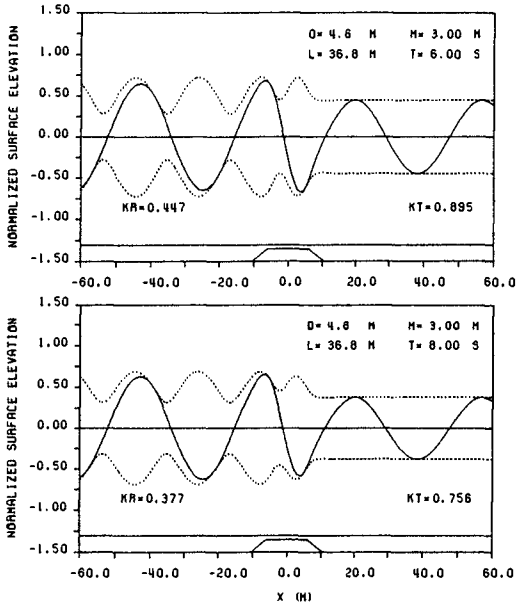


Figure 1. Wave field around Submerged breakwaters:
 (a) Impermeable; (b) Permeable.

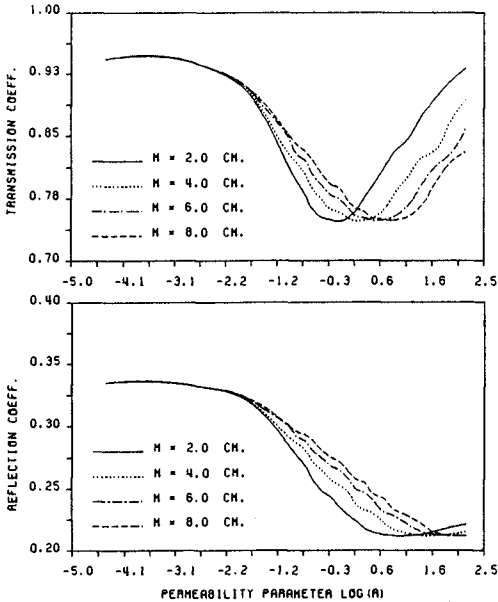


Figure 2. Transmission and reflection coefficients vs. R .
 (a) Transmission coefficient; (b) Reflection coefficient.

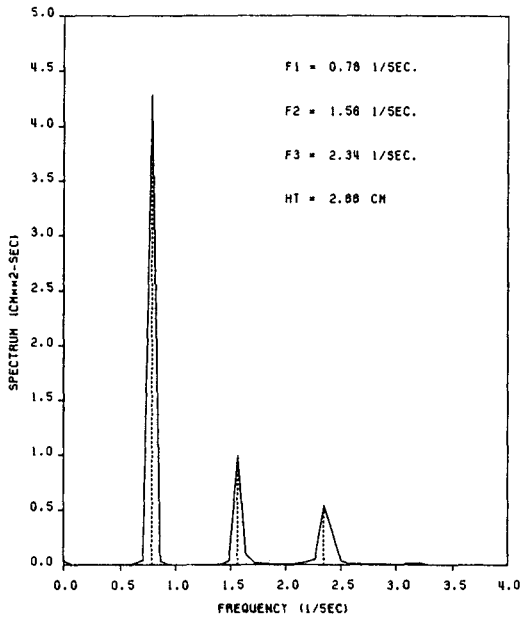


Figure 3. A typical power spectrum of transmitted waves

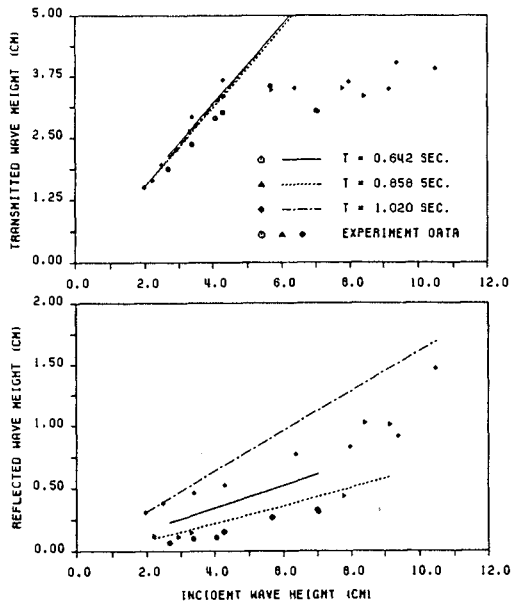


Figure 4. Transmitted and reflected wave height vs incident wave height.
 (a) Transmitted waves; (b) Reflected waves.

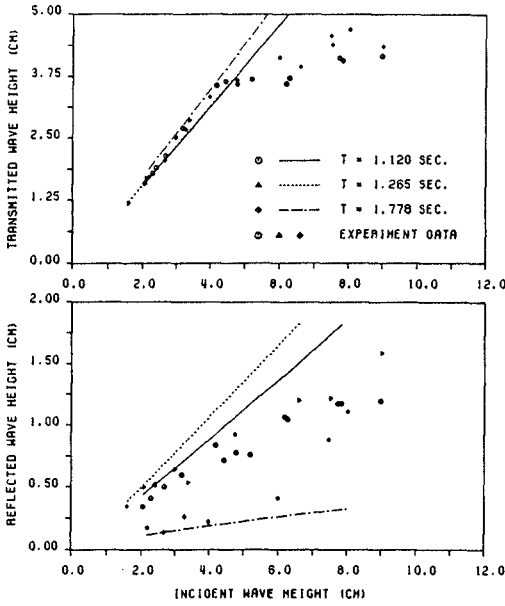


Figure 5. Transmitted and reflected wave height vs incident wave height. (a) Transmitted waves; (b) Reflected waves.

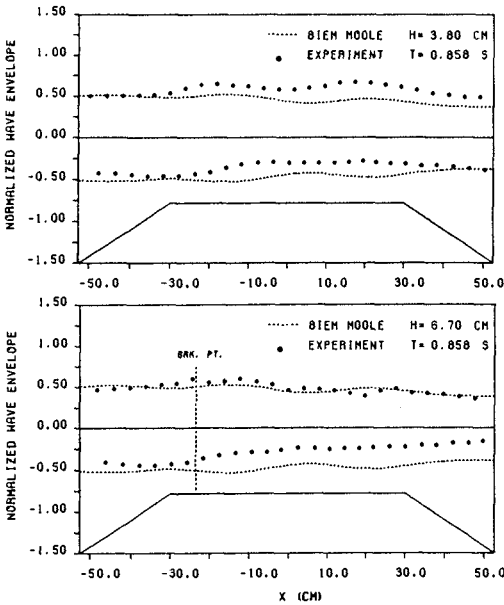


Figure 6. Comparison of measured and predicted wave envelopes. (a) non-breaking case; (b) breaking case